SUPERSONIC WING-NACELLE CONFIGURATION DESIGN USING AN UNSTRUCTURED ADJOINT METHOD

Hyoung-Jin Kim*[1], Shigeru Obayashi*[2], and Kazuhiro Nakahashi*[2]

비구조화 Adjoint 법을 이용한 초음속 날개-나셀의 공력설계

김 형진 [1]), Shigeru Obayashi[2]), and Kazuhiro Nakahashi[2])

3차원 Euler 방정식과 adjoint 법을 이용한 공력설계코드를 개발하였으며, 이를 초음속수송기의 주날개 설계에 적용하였다. 표면형상의 변화를 위해 Hicks-Henne 함수를 사용하였으며, 내부 격자점의 수정을 위해 타원형방정식법을 이용하였다. 나셀의 수직이동과 관련되지 않은 설계변수에 대해서는 내부격자점의 이동을 무시함으로써 계산시간을 크게 단축할 수 있었다. 양력과 날개단면두께를 일정하게 유지하면서 항력을 최소화하도록 단면형상을 최적화하였으며, 성공적인 결과를 얻음으로써 본 설계시스템의 타당성 및 효율성을 확인하였다.

Key Words: 초음속수송기(Supersonic transport), Adjoint method, 공력설계(aerodynamic design)

1. Introduction

With the advances in computational fluid dynamics (CFD) and computing power of modern computers, aerodynamic design optimization methods utilizing CFD codes are more important than ever. Among several design optimization methods applicable to aerodynamic design problems, the gradient-based method has been used most widely due to its well-developed numerical algorithms and relatively small computational burden. In the application of gradient-based methods to practical aerodynamic design problems, one of the major concerns is an accurate and efficient calculation of sensitivity derivatives of an aerodynamic objective function.

Sensitivity derivatives can be evaluated more robustly and efficiently by using a sensitivity analysis code based either on a direct method[1] or on an adjoint method[2-5]. An adjoint method is preferable in aerodynamic designs because it is more economical when the number of design variables is larger than the total number of an objective function and constraints. Reuther et al.[3], for example, designed aircraft configurations using a continuous adjoint method with the Euler equations in a structured multi-block grid system. Kim et al.[4] developed direct and adjoint sensitivity codes from 2-D Navier-Stokes code with an algebraic turbulence model in a structured grid system.

In this study, direct and adjoint sensitivity codes have been developed from a 3-D unstructured Euler solver based on a cell-vertex finite volume method. With the resulting adjoint code, aerodynamic design of

----
*1 한국항공우주연구소 터보기계연구그룹
   hyoungjin@kari.re.kr
*2 Dep't of Aero & Space Eng. Tohoku Univ., Sendai, 980-8579
   JAPAN

a Supersonic Transport (SST) wing with nacelle is conducted. Wing geometry is perturbed in an algebraic manner at five design sections. Interior grids are moved accordingly by the elliptic equation method. Grid sensitivities of interior nodes are neglected except those for design variables associated with nacelle translation in order to reduce required computational time for the mesh sensitivity calculation.

2. Flow Analysis

The Euler equations for compressible inviscid flows are written in an integral form as follows;

$$\frac{\partial}{\partial t} \int_{\Omega} Q dV + \int_{\partial\Omega} F(Q) \cdot n dS = 0 \qquad (1)$$

where $Q = [\rho, \rho u, \rho v, \rho w, e]^T$ is the vector of conservative variables; ρ the density; u, v, w the velocity components in the x, y, z directions; and e the total energy. The vector $F(Q)$ represents the inviscid flux vector and n is the outward normal of $\partial\Omega$ which is the boundary of the control volume Ω. This system of equations is closed by the perfect gas equation of state with a constant ratio of specific heats.

The equations are solved by a finite volume cell-vertex scheme. The control volume is a non-overlapping dual cell. For a control volume, Eq.(1) can be written in an algebraic form as follows;

$$V_i \frac{\partial Q_i}{\partial t} = -\sum_{j(i)} \Delta S_{ij} h^{n+1}\left(Q_{ij}^+, Q_{ij}^-, n_{ij}\right) \qquad (2)$$

where ΔS_{ij} is a segment area of the control volume boundary associated with edge connecting points i and j. This segment area ΔS_{ij} as well as its unit normal n_{ij} can be computed by summing up the contribution from each tetrahedron sharing the edge. The term h is an inviscid numerical flux vector normal to the control volume boundary, and $Q_{ij}^\pm$ are flow variables on both sides of the control volume boundary. The subscript of

summation, $j(i)$, means all node points connected to node i.

The numerical flux h is computed using an approximate Riemann solver of Harten-Lax- van Leer-Einfeldt-Wada(HLLEW)[6]. The second order spatial accuracy is realized by a linear reconstruction of the primitive gas dynamic variables $q = [\rho, u, v, w, p]^T$ inside the control volume using the following equation;

$$q(r) = q_i + \psi_i \nabla q_i \cdot (r - r_i), (0 \leq \psi \leq 1) \qquad (3)$$

where r is a vector pointing to point (x, y, z), and i is the node index. The gradients associated with the control volume centroids are volume-averaged gradients computed by the surrounding grid cells. Venkatakrishnan's limiter[7] is used for the function ψ_i in Eq.(3) because of its superior convergence properties.

In order to integrate Eq. (2) in time, the Lower-Upper Symmetric Gauss-Seidel(LU-SGS) implicit method[8] is adopted.

3. Sensitivity Analysis

3.1 Direct Method

An aerodynamic sensitivity analysis begins with the fact that the discrete residual vector of the non-linear flow equations is null for a converged flow field solution of steady problems, which can be written symbolically as

$$R_i[Q, X, \beta] = 0, \qquad (4)$$

where X is the grid position vector, β the vector of design variables. Equation (4) can be directly differentiated via the chain rule with respect to β to yield the following equation.

$$\frac{dR_i}{d\beta} = \left[\frac{\partial R_i}{\partial Q}\right]\left\{\frac{dQ}{d\beta}\right\} + \{C_i\} = 0, \qquad (5)$$

where $\left\{C_i\right\} = \left[\dfrac{\partial R_i}{\partial X}\right]\left\{\dfrac{dX}{d\beta}\right\} + \left\{\dfrac{\partial R_i}{\partial \beta}\right\}$.

This equation is the direct sensitivity equation for the flow variable sensitivity $\{dQ/d\beta\}$. The vector $\{C_i\}$ has no relation with the $\{dQ/d\beta\}$, and thus, is constant throuthout the solution process of the sensitivity equation for a design variable β. $\{dX/d\beta\}$ in the $\{C_i\}$ is a vector of grid sensitivity, which can be calculated by a finite-difference approximation or the direct differentiation of a routine for the grid generation or modification.

In order to find the solution $\{dQ/d\beta\}$ of Eq.(5) iteratively, a pseudo time term is added as follows to obtain the incremental form;

$$V_i\frac{\partial \mathbf{Q}_i'}{\partial t} = \left[\frac{\partial R_i}{\partial Q}\right]\left\{\frac{dQ}{d\beta}\right\}^{n+1} + \{C_i\}, \quad (6)$$

where Q' represents the solution vector $\{dQ/d\beta\}$. The above system of equations is solved with the LU-SGS scheme that is used for the flow solver.

When the flow variable sensitivity vector $\{dQ/d\beta\}$ is obtained, the total derivative of the objective function F can be calculated. The objective function F is usually aerodynamic coefficients such as C_D, C_L, C_M, or differences of surface pressures with specified target pressures. F is a function of flow variables $\mathbf{Q}$, grid position $\mathbf{X}$, and design variables β, i.e,

$$F = F\big(Q(\beta), X(\beta), \beta\big). \quad (7)$$

The sensitivity derivative of the cost function F with respect to a design variable β is given by

$$\left\{\frac{dF}{d\beta}\right\} = \left\{\frac{\partial F}{\partial Q}\right\}^T\left\{\frac{dQ}{d\beta}\right\} + \left\{\frac{\partial F}{\partial X}\right\}^T\left\{\frac{dX}{d\beta}\right\} + \left\{\frac{\partial F}{\partial \beta}\right\}, (8)$$

3.2 Adjoint Method

Since the total derivative of the flow equations in the steady state is null as can be seen in Eq.(5), we can introduce adjoint variables and combine Eqs. (5) and (8) to obtain

$$\left\{\frac{dF}{d\beta}\right\} = \left\{\frac{\partial F}{\partial Q}\right\}^T\left\{\frac{dQ}{d\beta}\right\} + \left\{\frac{\partial F}{\partial X}\right\}^T\left\{\frac{dX}{d\beta}\right\} + \left\{\frac{\partial F}{\partial \beta}\right\}$$
$$+ \{\lambda\}^T\left\{\left[\frac{\partial R}{\partial Q}\right]\left\{\frac{dQ}{d\beta}\right\} + \{C\}\right\}. \quad (9)$$

Coefficients of the flow variable sensitivity vector $\{dQ/d\beta\}$ form the following adjoint equation.

$$\left[\frac{\partial R}{\partial Q}\right]^T\{\lambda\} + \left\{\frac{\partial F}{\partial Q}\right\} = 0, \quad (10)$$

If one finds the adjoint variable vector $\{\lambda\}$ which satisfies the above adjoint equation, one can obtain the sensitivity derivative of F with respect to β without any information about the flow variable sensitivity vector $\{dQ/d\beta\}$. This makes the computational cost for the sensitivity analysis independent of the number of design variables. Equation (9) eventually becomes to the following form,

$$\left\{\frac{dF}{d\beta}\right\} = \left\{\frac{\partial F}{\partial X}\right\}^T\left\{\frac{dX}{d\beta}\right\} + \left\{\frac{\partial F}{\partial \beta}\right\} + \{\lambda\}^T\{C \quad (11)$$

Figure 1 compares a two-dimensional example of flux accumulation for the flow solver and the adjoint method. In the flow solver, primitive flow variables are reconstructed at the control volume surface using surrounding node point values. Then the flux $\mathbf{h}$ through the control volume surface is calculated and accumulated at both nodes 1 and 2. This is repeated for all edges to obtain flux residual for the control volume. On the other hand, in the adjoint method, the adjoint flux $[\partial R/\partial Q]^T\{\lambda\}$ is accumulated at all the node points that have effects on the reconstructed flow variables at the control volume surface. For example, if we set the flux for the edge connecting node 1 and node 2 as R_{12} ($= -\Delta S_{12}\mathbf{h}_{12}$), accumulation of the adjoint residual R_adj is made at nodes related with node 1 as follows.

$$R\_adj_j \Leftarrow R\_adj_j + \left[\frac{\partial R_{12}}{\partial Q_j}\right]^T \lambda_j, j = 1, 2, 3, ..,7 \quad (12)$$

For nodes surrounding node 2,

$$R\_adj_j \quad <= R\_adj_j - \left[\frac{\partial R_{12}}{\partial Q_j}\right]^T \lambda_j, j = 1, 2, 3, 7, 8, 9, 10.$$

This causes small loops for the neighboring nodes to be inserted into the big loop for all edges. The length of the small loop was usually from 5 to 25 around a node point for a three dimensional Euler grid depending on the grid structure. If the adjoint code is run on a vector machine, it would hamper the flux calculation routine of the adjoint code to be vectorized with the big loop of edges.
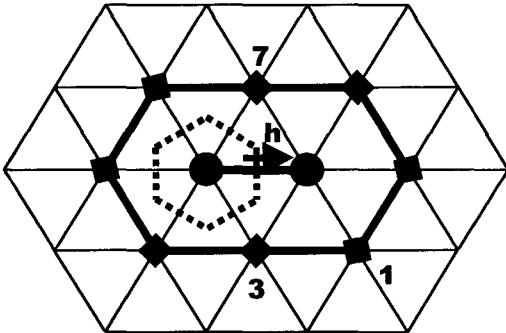

Fig.1 A 2-D example of flux accumulation for the flow solver and the adjoint method

In this study, the required differentiation process is conducted by human hand. Hand differentiation of a modern CFD code is somewhat a tedious job to do. However, if once done carefully, it provides an efficient sensitivity analysis tool.[4]

3.3 Sensitivity Code Validation

In order to validate the direct and adjoint sensitivity codes developed in this study, sensitivity analyses are conducted for a typical Supersonic Transport (SST) immersed in a supersonic flow. Flow conditions are $M_\infty = 2.0$ and $\alpha = 2.0$ degree. All the computations for the code validation were conducted with a single processor of a NEC SX-4 vector computer.

We used a simple wedge-type shape function for the purpose of test. The sensitivity derivatives are compared with those computed by the forward finite-

difference approximation with a step size $\Delta\beta$ of 10^{-7}. The residual of the flow solver is reduced to nearly machine zero for the finite difference calculation. Table 1 compares the sensitivity derivatives by the adjoint, direct, and finite-difference method. They compare very well with one another with errors less than 0.004 %.

Table 2 compares required memory and computational time for the Euler solver and its sensitivity codes. The required memory for both direct and adjoint codes seems to be reasonable. The adjoint code costs somewhat large computational time per iteration due to the poor vectorization performance of the adjoint residual accumulation routine as mentioned in the previous section. We also tested the ratio of computational time of the flow solver over the adjoint code at a Compaq α workstation, a scalar machine, and found that the adjoint code costs only 1.5 times the CPU time of the flow solver per iteration.

Table 1 Comparison of sensitivity derivatives: errors are with respect to the values of FD

	Finite Difference	Direct code (%error)	Adjoint code (%error)
$dC_L/d\beta$	1.308065	1.308050 (0.00115)	1.308056 (0.00069)
$dC_D/d\beta$	0.0983594	0.0983587 (0.000712)	0.0983557 (0.00376)

Table 2 Comparison of memory and CPU time; numbers in the parentheses are relative ratios to the flow solver

	Flow Solver	Direct code	Adjoint code
Required Memory (MB)	160	222 (1.39)	360 (2.25)
Time per Iteration (sec.)	3.75	5.7 (1.52)	26.5 (7.07)

4. Design Methodology

4.1 Design Objective

The present design method using the unstructured

Euler solver and the adjoint method is applied to an experimental SST wing with a flow-through type engine nacelle attached on its lower surface, which is under development by National Aerospace Laboratory of Japan as a basic study for the next generation supersonic transport.[9]

The objective of the present design study is defined as follows.

$$\text{Minimize } C_D \qquad (13)$$
$$\text{Subject to } C_L = C_L^*$$

where C_D and C_L are drag and lift coefficients, respectively, and C_L^* is specified. If the lift constraint is dealt as an explicit constraint in an optimizer, it requires an additional adjoint code computation for the C_L derivatives. In this study, therefore, the lift constraint is satisfied running the flow solver in a fixed-lift mode, in which the incidence angle α is adjusted based on $C_{L\alpha}$. Since we would like to minimize drag when $C_L = C_L^*$, i.e. at an adjusted incidence angle, the objective function $F = C_D$ should be modified as follows to consider the lift constraint consistently,

$$F = C_D - \frac{\left(\dfrac{\partial C_D}{\partial \alpha}\right)}{\left(\dfrac{\partial C_L}{\partial \alpha}\right)}\left(C_L - C_L^*\right) \qquad (14)$$

where C_D and C_L are drag and lift coefficients respectively without any incidence angle modification, and C_L^* is the target lift coefficeint, which is 0.100 for this case.

4.2 Design Parameters and Grid Modification Method

The wing section geometry is modified adding a linear combination of Hicks and Henne shape functions[10], We used five design sections along the SST wing span and defined 20 Hicks-Henne design variables and one twist angle per a design section. In addition to the 105 design variables, the height of diverter is also considered as a design parameter. With the new geometry of the design sections, node points on the wing surface are linearly interpolated.

When the surface grid is modified, the interior grid points should be moved accordingly. In the structured grid approach, the interior grid positions can be moved with a relative ease using an algebraic mesh movement strategy which modifies the grid point coordinates along a grid line of the same index. In the unstructured grid method, however, such a simple grid modification method cannot be applied, and a more sophisticated grid movement method is needed.

For the movement of the grid points with the perturbed surface grid, we used the elliptic partial differential equation method proposed by Crumpton and Giles[11]. In the method, the displacement δx from initial grid point x_0 is prescribed by the following equation with Dirichlet boundary conditions

$$\nabla \cdot \left(k\nabla \delta x\right) = 0 . \qquad (14)$$

Diffusion coefficient k is constant in each cell and is given by

$$k = \frac{1}{max(Vol, \varepsilon)}, \qquad (15)$$

where Vol is the control volume of each grid point and ε is a small positive number to prevent k from becoming negative. The elliptic equation (17) is discretized by a finite volume method, and subsequent linear algebraic equations are solved by the conjugate gradient method[12]. Required computational time to obtain converged solution δx was same with that of a few iterations of the Euler solver.

4.3 Grid Sensitivity

The elliptic equation method for the interior grid movement is differentiated to be applied to the grid sensitivity calculation for the vector {C} in Eq.(5) with respect to each geometric design variable. Since this requires almost the same computational cost with the grid movement procedure, the total computational burden would be a substantial amount if the number of design variables becomes large; say, more than one hundred.

One possible way to reduce the computational burden of the grid sensitivity calculation is to neglect the grid sensitivity of interior node points. Eyi and Lee[1] defined grid sensitivities on the body surface only by ignoring the movement of interior grid points in their study on direct sensitivity analysis with 2-D Euler equations. Although they did not present an explicit accuracy comparison, they reported that the simplification approach does not affect the accuracy of the resulting sensitivity.
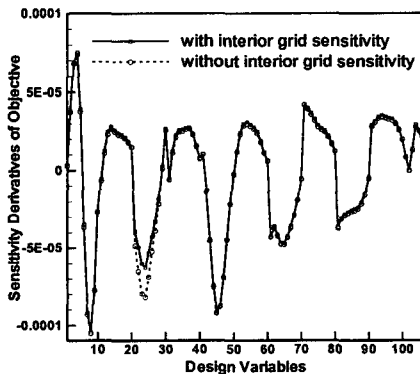

Fig.2 Comparison of sensitivity derivatives with and without interior grid sensitivity information

In this study, we made a comparison between the derivatives with and without the interior grid sensitivities in order to evaluate the accuracy of the simplification approach ignoring the interior grid movement. Figure 2 compares the derivatives of the objective function obtained with and without the interior grid sensitivity information. Derivatives with respect to the design variables have little difference between the two values except those of 21 ~ 30 in the design variables. The design variables with indices from 21 to 30 are defined on the lower surface of the second design section, which is located at the centerline of the diverter. Thus, they cause the nacelle to be translated vertically because of the constraint on the leading edge height which will be mentioned in a following section. It has been shown in Ref.2 that for geometries with singularity such as sharp trailing edges, interior mesh

sensitivities must be included for the calculation of the derivatives associated with translation. In this case, the nacelle inlet and outlet have sharp edges, which causes the derivatives calculated without interior mesh sensitivities to be deviated from those values obtained with the mesh sensitivities. It can be noted here that the interior grid sensitivities are required for design variables associated with translation of the nacelle, and, on the other hand, the grid sensitivities can be ignored for other ordinary design variables, i.e. coefficients of shape function or twist angles, without major accuracy degradation.

In this study, interior grid sensitivities for the ten design variables (21~30) are calculated by the elliptic equation method, while for other design variables, only the surface grid sensitivities are defined. This simplification approach required only a quarter of the computational time for the approach computing all the interior grid sensitivities.

4.4 Optimization Method

For the minimization of the objective function with specified constraints, the ADS(Automated Design Synthesis) program[13] was used as an optimizer. The Sequential Quadratic Programming (SQP) method is adopted in which the objective is approximated by a quadratic Taylor series expansion to create a direction-finding problem. This subproblem is solved using the Modified Method of Feasible Directions. Lagrangian multipliers are calculated at the optimum of the subproblem. Then one-dimensional search is conducted using quadratic polynomial interpolation. When the one design iteration is complete, the approximated Hessian matrix is updated by the Broydon-Fletcher-Goldfarb-Shanno formula.

5. Design Results

At the design conditions freestream Mach number is 2.0 and C_L is 0.100. Figure 3 shows the wing-nacelle configuration and surface grids of initial ge-

ometry. The number of nodes and cell of the volume grid are about 270,000 and 1,500,000, respectively.

In the present optimization the diverter leading edge height is also constrained to be larger than the initial value. This lower side constraint is to prevent the boundary layer flow from being entrained into the engine, which might occur if the height of the diverter leading edge becomes smaller than the initial value. Additional constraints are imposed so that wing section thickness values at front (5%chord), rear (80%chord) spar position and maximum thickness position (50 % chord) should be larger than those of the initial geometry.

The density residual of the Euler solver was reduced by four orders from the initial value, and that of the adjoint code by two orders. The SQP optimization iterations converged with three iterations to obtain a drag coefficient reduced by 16 counts from 0.0205 to 0.0189 retaining the lift coefficient as the specified value and satisfying imposed thickness constraints. Table 3 summarizes the design results. During the design process, the Euler solver was run three times and the adjoint code also three times, which is equivalent to about less than six analyses of the Euler solver in computational time.

Fig.3 Surface grids of NAL experimental supersonic aircraft with nacelles

Table 3 SST wing-nacelle design results

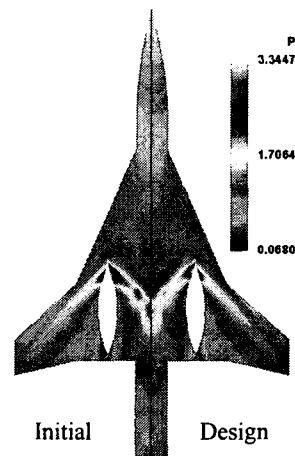|	Initial	Design	Δ (%)
C_L	0.10017	0.10020	+0.03
C_D	0.020513	0.018918	-7.78
L/D	4.883	5.297	+8.48

Initial   Design

Fig.4 Comparison of lower surface pressure contours
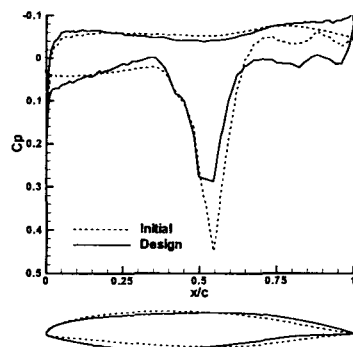

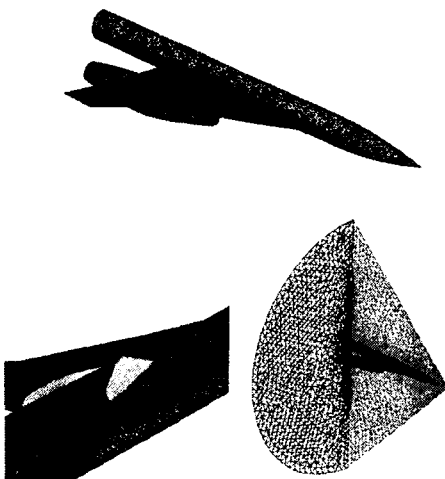Fig.5 Section shapes and pressure distributions at a design section(η=0.232); ---- initial, —design.

Figure 4 shows the surface pressure contours on the wing lower surface. It can be noted that the strength of the impinging shock wave on the wing lower surface generated by the diverter leading edge is greatly reduced through the design procedure. Also the strength of the expansion wave at the trailing edge of the diverter has been remarkably reduced. Figure 5 compares wing section shapes and pressure distributions at a design section. The wing section shapes are elongated by a factor of three in the normal direction.

Section pressure distributions also show that the shock strength on the lower surface has been remarkably reduced. The shock strength remains almost the same for additional design iterations, and it could be reduced more if there were no constraints on the wing section thickness.

The leading-edge height of the diverter remained the same as the initial value, since the gradient of the objective function with respect to the height is positive throughout the design iteration. This is quite natural in a sense that the volume of the aircraft will be increased and therefore the pressure drag will be increased if the diverter height increases.

6. Concluding Remarks

An aerodynamic design optimization system is developed using the unstructured Euler solver and the discrete adjoint method. Surface geometry is perturbed by simple algebraic shape functions and a twist angle variation. The interior grid position movement is made by the elliptic equation method. For an efficient calculation of terms related with the grid sensitivities, grid sensitivities of interior node points are ignored except those for the design variables associated with nacelle translation. The present method is successfully applied to design a SST wing with nacelles. The impinging shock wave from the diverter on the wing lower surface has been greatly reduced, and as a consequence, drag is remarkably reduced by three iterations of the SQP optimizer.

References

1. Eyi, S. and Lee, K. D., "Effect of Sensitivity Analysis on Aerodynamic Design Optimization," FED- Vol.232, CFD for Design and Optimization, ASME 1995.

2. Anderson, W. K., and Venkatakrishnan, V., "Aerodynamic Design Optimization on Unstructured Grids with a Continuous Adjoint Formula-

tion," AIAA 97-0643, 1997.

3. Reuther, J. J., Jameson, A., Alonso, J. J., Rimlinger, M. J., and Saunders, D., "Constrained Multipoint Aerodynamic Shape Optimization Using an Adjoint Formulation and Parallel Computers, Part 1," J. of Aircraft, vol. 36, No.1, pp51-60, 1999.

4. Kim, H. J., Kim, C., Rho, O. H., and Lee, K., "Aerodynamic Sensitivity Analysis for Navier-Stokes Equations," AIAA 99-0402, Jan. 1999.

5. Sung, C.-H. and Kwon, J.H., "Accurate Aerodynamic Sensitivity Analysis Using Adjoint Equations," AIAA J. Vol.38, No.2, pp.243-250, 2000.

6. Obayashi, S., and Guruswamy, G. P., "Convergence Acceleration of an Aeroelastic Navier-Stokes Solver", AIAA J. Vol.33, No.6, pp.1134-1141, 1995.

7. Venkatakrishnan, V., "On the Accuracy of Limiters and Convergence to Steady State Solutions," AIAA Paper 93-0880, January 1993.

8. Yoon, S. and Jameson, A., "Lower-Upper Symmetric-Gauss-Seidal Method for the Euler and Navier-Stokes Equations," AIAA J., Vol.26, No.9 pp. 1025-1026, 1988.

9. Iwamiya, T., "NAL SST Project and Aerodynamic Design of Experimental Aircraft," Proc. Computational Fluid Dynamics '98, Vol.2, ECCOMAS 98, John Wiley & Sons, Ltd. pp.580-585, 1998.

10. Hicks, R. M. and Henne, P. A., "Wing Design by Numerical Optimization," J. of Aircraft, Vol.15, No.7, pp. 407-412. 1978.

11. Crumpton, P. I. and Giles, M. B. "Implicit Time Accurate Solutions on Unstructured Dynamic Grids," AIAA 95-1671, June 1995.

12. Press, W. H., Teukolsky, S. A., Vetterling, W. T., and Flannery, B. P., "Numerical Recipes in Fortran," 2nd ed. Cambridge Univ. Press, Cambridge, England, UK, 1992.

13. Vanderplaats, G. N., "ADS – A Fortran Program For Automated Design Synthesis version 3.00," Engineering Design Optimization, INC., 1987.